

Diameter-controlling growth of solid-cored carbon nanofibers on a pulse plated iron nanocrystalline substrate in flames

Yueli Liu^a, Chunxu Pan^{b,c,**}, Wen Chen^{a,*}

^a State Key Laboratory of Advanced Technology for Materials Synthesis and Processing, and School of Materials Science and Engineering, Wuhan University of Technology, Wuhan 430070, People's Republic of China

^b Department of Physics, Wuhan University, Wuhan 430072, People's Republic of China

^c Key Laboratory of Acoustic and Photonic Materials and Devices of Ministry of Education, Wuhan University, Wuhan 430072, People's Republic of China

Received 24 September 2007; received in revised form 5 February 2008; accepted 5 February 2008

Available online 12 February 2008

Abstract

A novel process was introduced in this paper for the diameter-controlling synthesis of carbon nanofibers (CNFs) in the ethanol flames. The carbon nanofibers were grown on a nanocrystalline Fe layer, which was electro-deposited on a substrate using periodic reverse (P.R.) pulse plating. It was found that the quality of the plating nanocrystalline and the corresponding carbon nanofibers was related with two plating parameters: output pulse frequency (f) and duty cycle (r). In addition to that the straight and helical carbon nanofibers were selectively synthesized by addition of different additives in plating bath. In this paper, the base-growth mechanism of carbon nanofibers was clearly discussed.

© 2008 Elsevier Ltd. All rights reserved.

Keywords: A. Nanostructures; A. Thin films; B. Crystal growth

1. Introduction

Generally, the fiber-like nanostructures indicate both carbon nanotubes (CNTs) and carbon nanofibers (CNFs) with or without a hollow core when its diameters are in the range of 50–200 nm [1–4]. Chemical vapor deposition (CVD) process is considered as an effective method to grow vapor-grown carbon nanofibers (VGCNFs), which are obtained by the following processes: a hollow and high-crystallinitic graphite carbon nanotubes were formed in the inner region, and then a low degree of graphitic pyrocarbon layer was deposited on the nanotubes as a surrounding layer [5–7]. However, according to the growth mechanism, a filament with or without the central hollow core indicates the different materials with various characteristics and properties [8].

It is quite important how to prepare uniform and fine metal catalyst, which may determine the size and structure of resultant carbon nanofiber in the catalytic CVD synthesis [9–12]. Non-supported metal catalyst for CNF growth has been reported to be prepared through the precipitation of metal carbonate by calcined to metal oxide, which is reduced to metal by reaction with the carbon source gas [9,10]. In other side, metals or their alloys have been often used in

* Corresponding author. Tel.: +86 27 8765 1107; fax: +86 27 8786 4580.

** Corresponding author. Tel.: +86 27 8721 4880; fax: +86 27 6875 2569.

E-mail addresses: chenw@whut.edu.cn (W. Chen), cspan@whu.edu.cn (C. Pan).

supported form on Al_2O_3 , SiO_2 , TiO_2 , zeolite, and carbon black (CB) substrates [11,12]. However, the removal of those oxides of the substrates or the catalysts must be considered, and their burdensome purification under severe conditions would greatly influence CNF costs.

In our previous work [8], CNFs' diameter varies in a wide range of 20–250 nm because the pretreatments on the sampling surface of the substrates are roughly controlled by mechanical grinding, polishing or etching. The main reasons for these pretreatments are difficult to produce the catalysts with the desired particle size, dispersion of the substrate, and also influence the repeatability during the synthesizing process.

Pulse plating has been developed as a regular technique for synthesizing metal nanocrystallites with grain size in the range of 6–100 nm by adjusting plating parameters [13–18]. In the previous work [19], we proved that the nickel (Ni) nanocrystalline layer plated on the substrate adopted as catalyst to grow hollow-cored CNTs in the ethanol flames, and it is also an effective method for controlling the CNTs diameters through the controlling of grain size of the plating by adjusting the plating parameters, such as output pulse frequency (f) and duty cycle (r).

The present work also adopts the similar route as described in the previous work [19], i.e., iron (Fe) nanocrystalline layer was deposited on the surface of the substrate and controlled the growth rate of solid-cored CNFs from the ethanol flames. It is expected that the grain size of catalyst particles is not only adjusted by the plating parameters, but also becomes uniform, which can favor to control the diameter and uniformity of the CNFs by using the nanocrystalline catalyst in the present process.

2. Experimental

A numerical control double pulse (square-wave pulse) plating electric source (GKDM 30-15, Xin Du, China) is used for preparation of iron nanocrystalline layer during this experiment. The size of anode iron foil is 50 mm × 50 mm with purity of 99% and above. The cathode is made of pure copper (Cu) substrate with a size of 30 mm × 30 mm, which is mechanically polished for certain roughness, or treated with mirror finish before plating.

Ferrous chloride ($\text{FeCl}_2 \cdot 4\text{H}_2\text{O}$) 380 g/L, boric acid (H_3BO_3) 20 g/L, saccharin ($\text{C}_7\text{H}_5\text{NO}_3\text{S}$) 5 g/L and sodium fluoride (NaF) 2.5 g/L are used for proposing bath composition. The pH value (2.0) of the electrolyte is adjusted by adding sulfuric acid (H_2SO_4) and potassium hydroxide (KOH). The working time for positive and negative pulses is 8 T and 2 T (pulse cycle $T = t_{\text{on}} + t_{\text{off}}$). The average applied current of positive electrode and negative electrode is 0.5 and 0.3 A, respectively. The electro-deposition process is carried out at room temperature. The maintained time for plating is 5 min. The clear details are listed in Table 1.

In order to obtain the requisite plating layer, the output pulse frequency and duty cycle are chosen in two sets:

- (1) Duty cycle 10% with frequencies 10, 20, 50, 100, 200, 500, 1000 and 2000 Hz;
- (2) 50 Hz frequency with duty cycles 5%, 10%, 20%, 50%, and 90%.

The solid-cored CNFs were synthesized by a common ethanol flame with absolute ethanol ($\text{C}_2\text{H}_5\text{OH}$). The plated substrates were inserted into the ethanol flame and kept there for 20 min for the deposition of carbonaceous materials as black layer on the surface of the substrates.

Table 1
The bath compositions and pulse plating conditions

Composition or parameter	Data
Ferrous chloride ($\text{FeCl}_2 \cdot 4\text{H}_2\text{O}$)	380 g/L
Boric acid (H_3BO_3)	20 g/L
Saccharin ($\text{C}_7\text{H}_5\text{NO}_3\text{S}$)	5 g/L
Sodium fluoride (NaF)	2.5 g/L
PH value	2.0
Positive pulse work time	8 T
Negative pulse work time	2 T
Average voltage of positive	10 V
Average voltage of negative electrode	5 V
Bath temperature	24 °C

The morphologies and microstructures of the plated layers and CNFs were characterized by using a field emission gun scanning electron microscope (FEG-SEM) (SIRION, FEI, The Netherlands) and transmission electron microscope (TEM) (JEM2010, JEOL, Japan). The grain size and crystal lattice of the plated layer were measured by using an X-ray diffractometer (XRD) (D8 Advanced XRD, Bruker AXS, Germany). The laser Raman spectrum (1000, Renishaw, England) was used for the back-scattering configuration at room temperature. The excitation source was 514.5 nm Ar-ion laser lines. The laser line was in the range of 80–4500 cm^{-1} . A microscope objective of $\times 50$ was used in the laser beam. The spectral resolution was 3 cm^{-1} and the optical power was maintained at 5 mW on the sample.

In order to more precisely and correctly show the variation trend between the grain size of the plating and CNF diameter with the plating parameters, the error bar was marked on each result. Generally, the total relative error (u_t) includes the relative uncertainty (u_R) caused by the measurement process during the experiment and the accuracy of the apparatus (u_{App}).

The Laue method considers all of the diffraction contribution of the grains. Hence, in the present work the Laue breadth (B_s) was used instead of regular FWHM ($B_{1/2}$) in the Scherrer formula to calculate the grain size of the plating. The average value of all diffraction peaks is adopted in the present work, and their relative error is calculated. The accuracy of the X-ray diffractometer u_{XRD} is about 0.01% given by the machine manufacturer.

The CNFs diameter was statistically estimated from hundreds of CNFs in TEM images, and each CNF diameter was measured for 3–10 times. Therefore, the relative uncertainty u_R for each fiber was given in the diameter distribution range. The TEM error mostly comes from the magnification error caused by hysteresis effect. It is generally less than 0.5%.

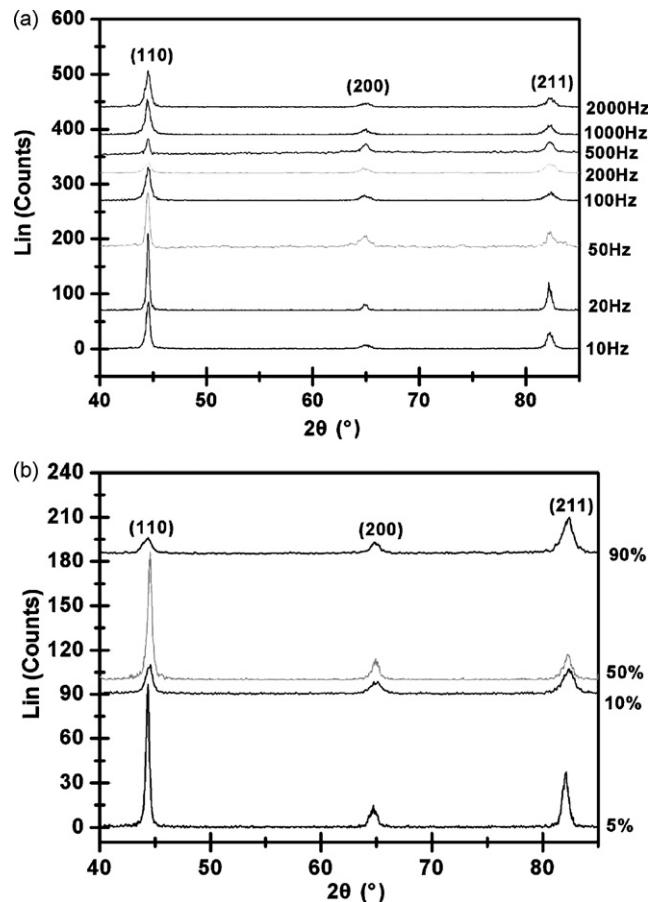


Fig. 1. XRD pattern of the plating layer on the copper substrate: (a) variant output pulse frequencies with a given duty cycle of 10%; (b) different duty cycle with a given pulse frequency of 50 Hz.

3. Results and discussion

3.1. Characterization of the nanocrystalline Fe layer

Fig. 1 shows XRD patterns of the plated Fe nanocrystalline layer having two sets of parameters. According to the Scherrer formula, the average grain size of the crystalline was calculated from the Laue breadth (B_s) of the diffraction peaks, as shown in Fig. 2. Fig. 2 reveals that the grain size of the plating layers is varied according to the plating condition and the relative error is less than 2.0%. Here the observed trend is reasonable and acceptable. The smallest grain size is formed at the frequency 100 Hz or duty cycle 10%. When the frequency is greater than 500 Hz, the grain size is decreased upto 1000 Hz and after that it is increased, as the too high or low frequency does not favor to growth the fine grain size and microstructure of the plating film instead of cracked morphology. It supports previous results obtained on nanocrystalline nickel plating [19].

Fig. 3 shows a typical SEM image of the plated nanocrystalline iron layer at 100 Hz output frequency and 10% duty cycle. The sizes of the grains are found to be 35–45 nm, which has good agreement with the results obtained by XRD pattern as shown in Fig. 2.

Generally, the effect of mass transport and double layer charging during pulse plating not only limit the accessible parameter space but also influence greatly on the microstructures and grain sizes of the deposits [13–18]. According to the electro-crystallization theory [18], the grain size r_c has an inverse proportion relationship with the current density (i) and overpotential (η). With the increasing of output pulse frequency, the overpotential (η) on the surface decreases,

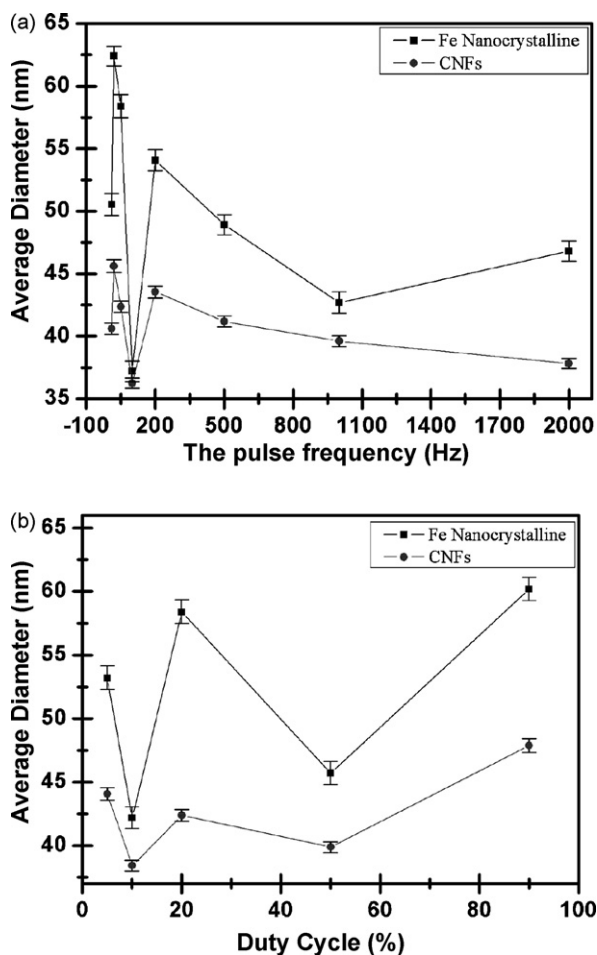


Fig. 2. The relationship between average sizes of the nanocrystalline Fe and CNFs and plating conditions: (a) output pulse frequencies; (b) duty cycle.

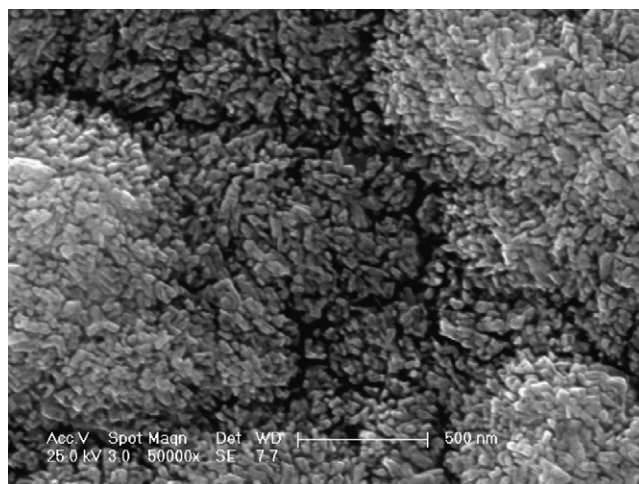


Fig. 3. SEM morphology of the iron plated nanocrystalline layer on a copper substrate at the output frequency 100 Hz and duty cycle 10%.

however, the current efficiency increases in the high frequency range (500 Hz) and decreases in the low frequency range [18].

When the pulse frequency is below 20 Hz, both of the surface overpotential and current efficiency are decreased simultaneously with increasing of pulse frequency due to the decreasing of current density. Here the grain size is increased with the increasing of pulse frequency. However, when the pulse frequency is increased above 200 Hz, the current efficiency is originated from double layer effect and it plays a dominant role for the grain growth. Moreover, the current efficiency will increase with increase of pulse frequency f when the f is over 500 Hz [18]. Therefore, the grain size decreased with the increasing of pulse frequency over 200 Hz in the present process. In the range of 20–200 Hz, the grain size decreased firstly and then increased with the increasing of pulse frequency [18,19], which is due to the contrary relationship between the surface overpotential (η) and current efficiency of the double layer effect. This is similar with the trend of copper nanocrystalline by pulse plating [20]. Therefore, Fig. 2(a) experimentally exhibits that the grain sizes are changed due to surface overpotential and current efficiency in different output pulse frequency ranges [18]. Hence, the grain size of the plating layer can be controlled by output pulse frequency adjustments.

It is well known that the peak current density increases with the decrease of duty cycle at a definite average current density when the output pulse frequency is given [18,19]. Therefore, the grain size becomes smaller with decrease of duty cycle. When duty cycle is larger than 50%, then the on time is longer than the off time. It is not suitable for dispelling the concentration polarization. When the duty cycle is small at a given output pulse frequency, the work time of a pulse is shorter than the charge time of the cathode [21,22]. Similar to the plating Ni nanocrystalline, too small or large duty cycles are not the acceptable conditions during the plating process [18,19,21,22], as shown in Fig. 2(b). In practice, the optimal duty cycle is selected as 10%.

In present work, we conclude that 100 Hz output pulse frequency with duty cycle of 10% is the optimal condition parameters. The frequencies above 500 Hz with duty cycle at 20% are also acceptable.

3.2. Synthesis of the solid-cored CNFs

Generally, the diameter of CNFs is related with the size of catalysts [10,23,24]. It is found that the most CNFs diameters are in the range of 35–55 nm. Corresponding to the plated layers in Fig. 1, the variation of CNFs' average diameters with the plating conditions in Fig. 2 is statistically estimated from the TEM images, as shown in Table 2. The relative error is less than 1.1%, which shows the variation trend between the CNFs diameter and plating parameters is in the acceptable range. It is interesting to note that the variation tendency of the CNFs diameters is almost similar with the variation of grain sizes of the plated layers as shown in Fig. 2. However, the CNFs diameters are totally smaller than the nanocrystalline Fe grain sizes. Normally, the mean diameter of the CNFs matches that of the original catalyst particles [10,23]. However, the relationship between the CNFs diameter would be related with the location of the catalyst particle in the CNFs, which is originated from the growth model [24]. For example, in the tips of the CNFs, the

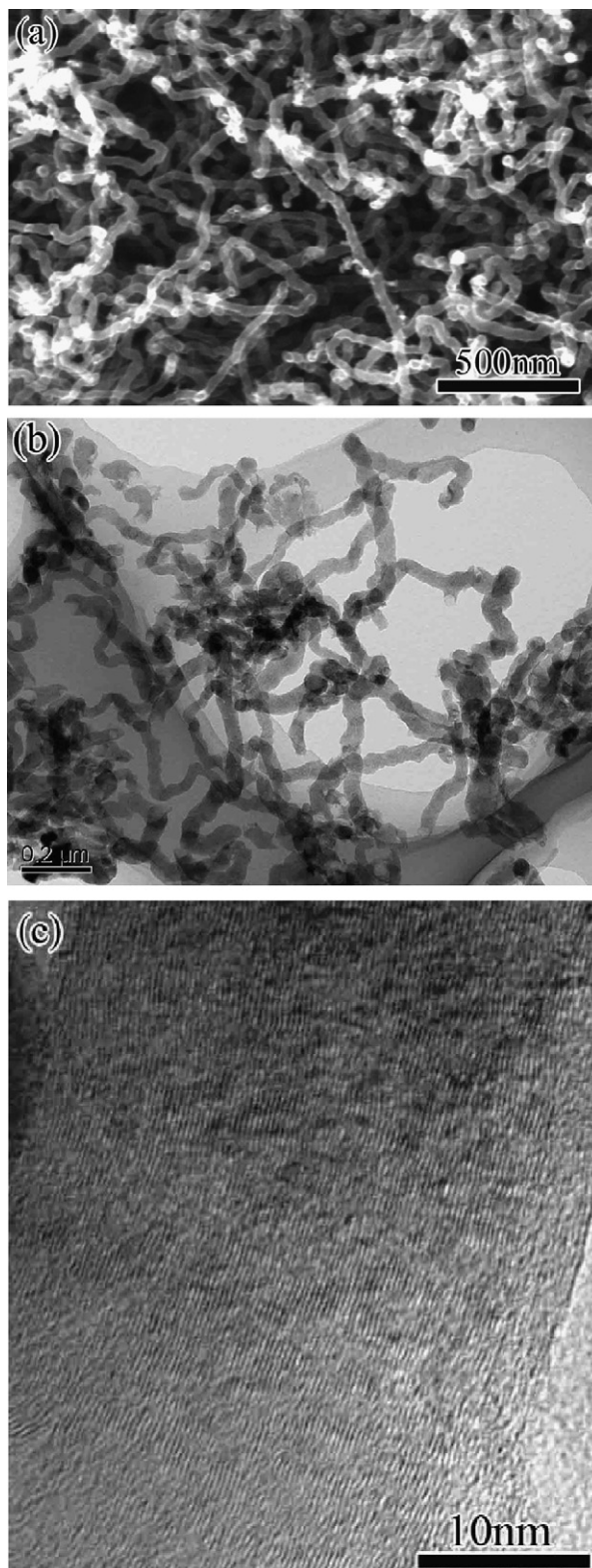


Fig. 4. Typical morphologies of the solid-cored CNFs: (a) SEM image; (b) TEM image; (c) HRTEM image.

Table 2

CNFs diameter distributions corresponding to different plating parameters of in two sets: (1) duty cycle 10% with frequencies 10, 20, 50, 100, 200, 500, 1000 and 2000 Hz; (2) 50 Hz frequency with duty cycles 5%, 10%, 20%, 50%, and 90%

Parameter	Range (%)							
	0–10 nm	10–20 nm	20–30 nm	30–40 nm	40–50 nm	50–60 nm	60–70 nm	70–80 nm
f (10 Hz)	1.33	3.56	15.11	24.00	25.33	13.78	11.11	5.78
f (20 Hz)	2.17	3.10	9.60	14.86	20.43	25.08	11.46	13.30
f (50 Hz)	0.42	3.05	11.51	14.30	26.99	25.73	9.41	8.59
f (100 Hz)	0.10	1.61	20.65	34.19	26.77	11.94	3.55	1.19
f (200 Hz)	0.10	1.79	7.68	27.14	33.75	19.46	7.32	2.76
f (500 Hz)	0	0.10	12.43	30.12	26.33	18.05	7.40	5.57
f (1000 Hz)	0	1.37	21.92	28.31	17.81	21.92	6.85	1.82
f (2000 Hz)	0	2.11	23.47	36.85	23.47	10.32	3.29	0.49
r (5%)	0	0.39	6.61	27.43	34.24	20.43	6.42	4.48
r (10%)	0	0.15	15.10	43.61	28.66	8.47	3.08	0.93
r (50%)	0	0.71	11.56	44.81	29.95	9.43	2.36	1.18
r (90%)	0	0.38	1.53	15.27	31.68	34.73	12.60	3.81

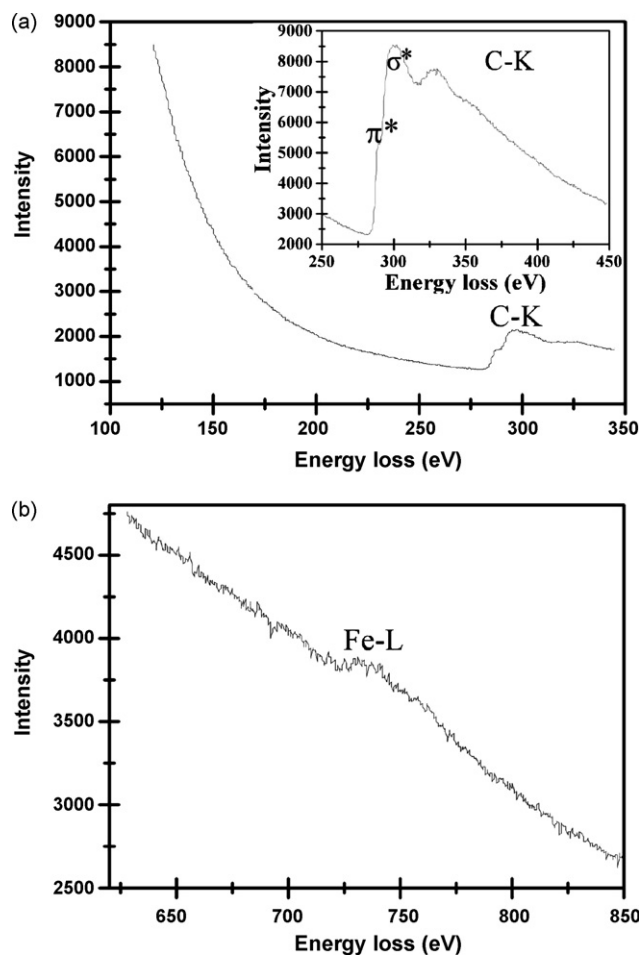


Fig. 5. EELS pattern of an individual CNFs: (a) B-K and C-K edge (the magnified C-K edge insetted); (b) Fe-L edge.

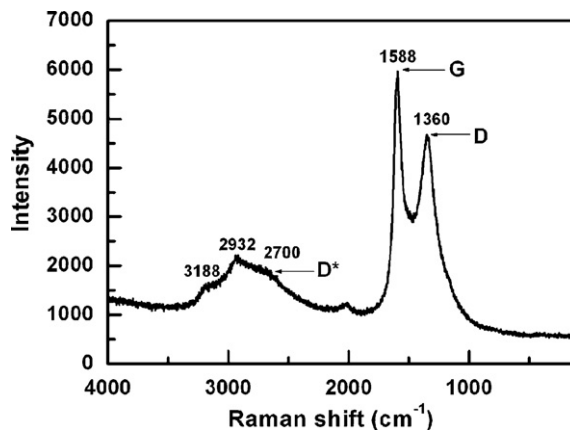


Fig. 6. Typical Raman spectrum of the solid-cored CNFs.

size of the catalyst particles is bigger than the diameter of CNFs, however, the size of the catalyst particles is smaller than the CNFs diameter when the catalyst particles is located at the tips, which is covered with the carbon layers [24]. In the present model, the catalyst of plating Fe nanocrystalline is closely coherent with the substrate and mostly only the upper portion of the sphere-like particles is exposed to act as the catalyst site for the CNFs growth. Therefore, the CNFs sizes are smaller than the nanocrystalline Fe grain sizes due to the growth model [19].

From the above results, it could be concluded that the plated nanocrystalline iron (Fe) grains used as catalyst particles played a key role for high quality solid-cored CNFs synthesis such as narrow diameter variation and high order microstructures, because the plating technique provided a more precise process to control the nanocrystalline

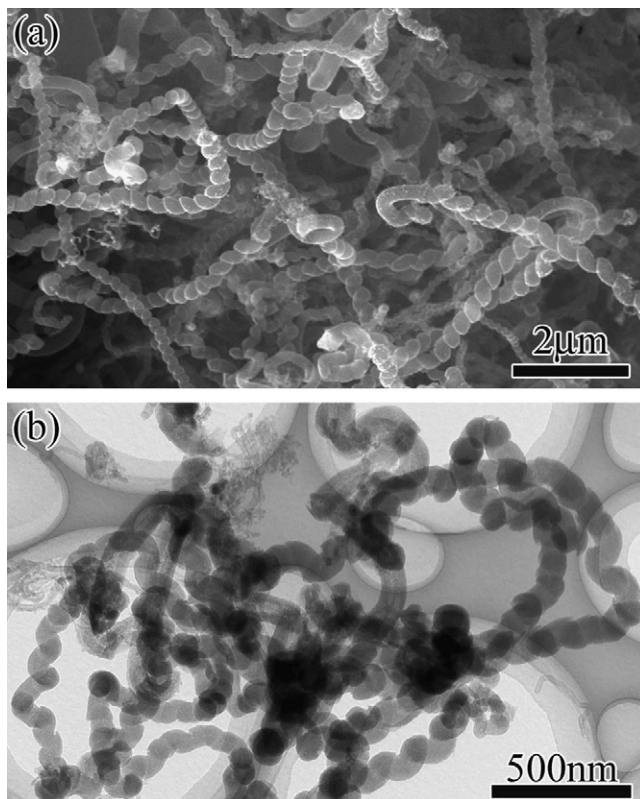


Fig. 7. Typical morphologies of the helical CNFs: (a) SEM image; (b) TEM image.

grain size and homogeneity and higher catalytic activity. In addition, the present process also provides a controlling diameter possibility of CNFs growth by adjusting the pulse plating parameters.

Fig. 4(a) shows that SEM image of the combustion carbonaceous materials has homogenous fibrillose structure gone with straight while non-uniform on the substrates. No particles are embedded at the end of fibers. Further TEM observations reveal that the fiber has solid-cored interior structure, which is different from the regular carbon nanotubes (CNTs), and most of them are in the range of 30–50 nm, as shown in Fig. 4(b). The images of CNFs are obtained by using high resolution transmission electron microscopy (HRTEM) as shown in Fig. 4(c). Compared with the previous work [8], the degree of order and graphitization of the CNFs in this method are highly improved. Electron energy loss spectroscopy (EELS) pattern shows that an intensified π -electron plasmon peak locates at 289 eV and the core-loss spectrum is similar with that of amorphous carbon, as shown in Fig. 5(a), which is the characteristic peak of

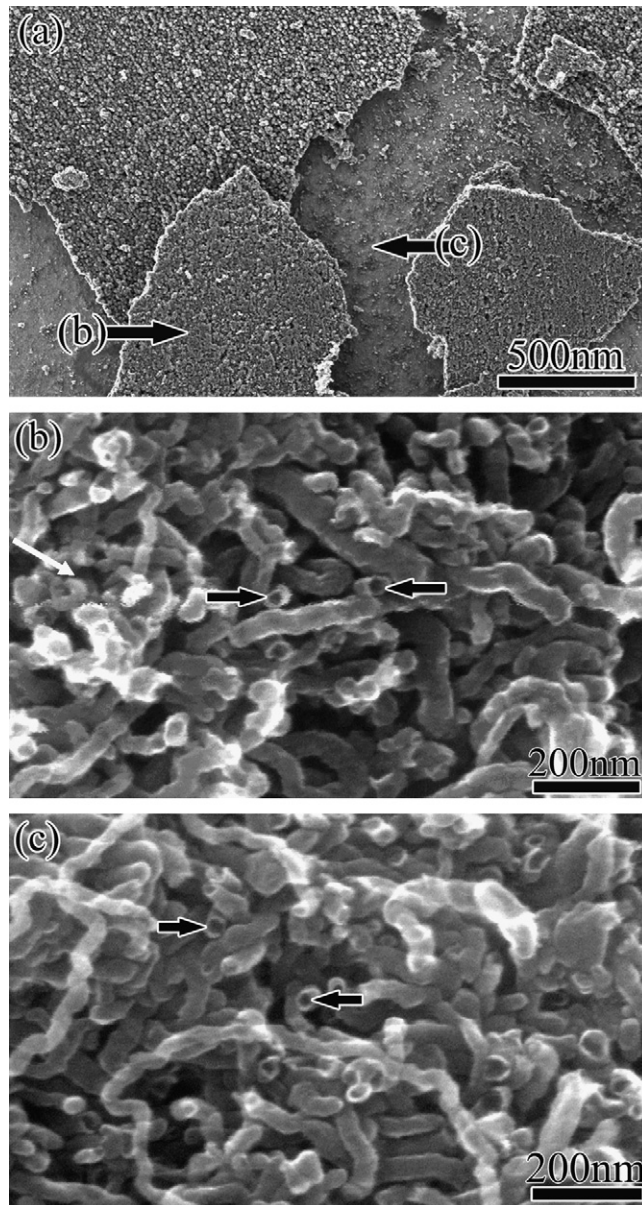


Fig. 8. SEM morphologies of the broken CNFs: (a) full view; (b) reverse side; (c) residual portion on the substrate (arrows indicate the broken CNFs).

the solid-cored CNFs [25]. The area of B-K edge is smooth without any peak, which reveals that the boron element do not exist in the present CNFs. The Fe-L edge with broadened peak still weakly exists at about 721.0 eV in Fig. 5(b), and it shows that the small amount of the Fe substance formation exists, which perhaps originates during the diffusion process of the carbon atom in the present growth model.

Fig. 6 shows a laser Raman spectrum of the solid-cored CNFs. Two typical peaks, i.e., D-band (1360 cm^{-1}) and G-band (1588 cm^{-1}), are observed. The intensity ratio I_D/I_G is about 0.73. In the previous work, we find the CNFs diameters are in range of 20–250 nm and intensity ratio I_D/I_G is 1.24 [8]. Therefore, the present CNFs exhibit a relatively higher degree of order and graphitization, which are in accord with the HRTEM results as shown in Fig. 4(c). However, the degree of order and graphitization of the CNFs in the present process is still low due to the presences of some amorphous carbon materials in CNFs. The reason for this lies in the low synthesizing temperature of $760\text{ }^\circ\text{C}$ in the ethanol flames [8].

In the present process, the helical CNFs are also synthesized when extra additives are added, such as sodium dodecyl sulphate ($\text{C}_{12}\text{H}_{25}\text{NaO}_4\text{S}$) and fluoroboric acid (H_3BO_3), as shown in Fig. 7. In general, the growth mechanism of helical CNFs is related with the widely accepted theory that ‘anisotropy of carbon deposition’, i.e., the capability of the carbon deposition and condensation is not same for all the crystal planes, and also for the coiled CNFs formed along with some of the orientation of the crystal planes [26–28]. In the present work, the additives are used for controlling the microstructures, properties of the plated materials and current distribution [29]. The helical or straight CNFs are produced based on the variations in crystallography of the plated nanosized grains or particles with the additional additives. Therefore, the present work also explores a novel route to control the CNFs growth and morphology. The detailed relationships among crystallography of plated layer, plating parameters and additives are still unclear. Further research work is to be undertaken.

The present solid-cored CNFs growth mechanism is different compared to the other methods, such as CVD process, etc. [5–7]. According to the previous work [8], it has been found that Ni and its compounds play a key role in the growth of ‘hollow-cored’ CNTs, Fe and its compounds have the effect in a novel solid-cored with less-ordered CNFs during ethanol flame synthesizing. The models of ‘hollow-cored mechanism’ and ‘solid-cored mechanism’ are given explanation for the formations of CNTs and CNFs, respectively. In this formations the enthalpy difference ΔH_f^0 for the carbides Fe_3C ($+4.7 \pm 1.1\text{ kJ/mol}$) and Ni_3C ($+1.2 \pm 1.3\text{ kJ/mol}$) are considered [30]. Here the energy of interaction increases in the order of $\text{Ni-C} < \text{Fe-C}$ [30–33]. Moreover, the existing of lattice shrinkage at certain higher temperatures suggests that the partial dissociation of carbon atoms from the carbides [33]. Therefore, Fe has a strong electron affinity with carbon and Ni has a weak electron affinity with carbon’, i.e. the pyrolyzed carbon atoms can be easily deposited and diffused in iron-contained particles due to affinity phenomenon, and then form the solid-cored CNFs.

In the present process, the plated nanocrystalline iron grains are used as catalysts for growing CNFs to form a strong interaction with the substrate. Hence, the grains are very close to contact with the substrate during CNFs growth. Fig. 8 shows the morphologies of the CNFs root portion with the substrate. Strictly speaking, the broken CNFs are observed from the combustion carbonaceous film as well as the residual portion of CNFs on the substrate, as indicated in Fig. 8(b and c).

Therefore, the present CNFs growth according to a base model has been described at the reference [34,35]. It may be noted that at initial stage, the carbonaceous gas decompose on the front-exposed surfaces of the iron particles when carbon atoms are dissolved in the particles. During the CNFs nucleation process, the dissolved carbon atoms diffuses through the particles and the diffusion of carbon atoms through iron particles is continuous so that it precipitates quickly so as to be continuously added to form the solid-cored CNFs [24]. That is why iron atom has a strong electron affinity to carbon atom, which results in large driving force and concentration of carbon atom by diffusing active carbon atoms. Therefore, the pyrolyzed carbon atoms can be easily deposited on the surface of the iron particles and diffused through the interior particles, and then they would form the solid-cored CNFs [8].

4. Conclusion

The plated nanocrystalline Fe layer was influenced by the output pulse frequency (f) and the duty cycle (r). The experimental results showed that the frequency 100 Hz and the duty cycle 10% were the optimal conditions for this process. The homogeneously sized CNTs were synthesized on the plated substrates in the ethanol flames. Compared with the traditional method, the present novel process is an effective method for controlling the CNFs diameter and the

grain size of the plated iron nanocrystalline by adjusting the plating parameters. Moreover, the straight or helical solid-cored CNFs were synthesized by addition of additives in the plating bath solution. The present CNFs were grown using base-growth mechanism on the plated substrates.

Acknowledgements

This work was supported by China Postdoctoral Science Foundation of PR China (CPSF) (No. 20060400254), the National Nature Science Foundation of China (Nos. 50672071, 50672072), the Key Project of Chinese Ministry of Education (105124), the Program for Changjiang Scholars and Innovative Research Team in University, Ministry of Education, China (PCSIRT) (No. IRT0547) and the Foundation for Innovation Research Team of Hubei Province (No. 2005ABC004). We would like to thank Dr. Jianbo Wang (Department of Physics, Wuhan University) for his excellent technical assistance on EELS characterizations.

Appendix A. Supplementary data

Supplementary data associated with this article can be found, in the online version, at [doi:10.1016/j.materresbull.2008.02.004](https://doi.org/10.1016/j.materresbull.2008.02.004).

References

- [1] S. Collins, R. Brydson, B. Rand, *Carbon* 40 (2002) 1089–1100.
- [2] H. Terrones, T. Hayashi, M. Muñoz-Navia, M. Terrones, Y.A. Kim, N. Grobert, R. Kamalakaran, J. Dorantes-Dávila, R. Escudero, M.S. Dresselhaus, M. Endo, *Chem. Phys. Lett.* 343 (2001) 241–250.
- [3] M. Endo, H.W. Kroto, *J. Phys. Chem.* 96 (1992) 6941–6944.
- [4] V.I. Merkulov, A.V. Melechko, M.A. Guillorn, D.H. Lownders, M.L. Simpson, *Appl. Phys. Lett.* 80 (2002) 476–478.
- [5] J. Mahalingam, C. Ramesh, K.G. Santosh, D. Kunzru, *Carbon* 33 (1995) 253–258.
- [6] M. Endo, K. Takeuchi, T. Hiraoka, T. Furuta, T. Kasai, X. Sun, C.-H. Kiang, M.S. Dresselhaus, *J. Phys. Chem. Solids* 58 (1997) 1707–1712.
- [7] Y.Y. Fan, H.M. Cheng, Y.L. Wei, G. Su, Z.H. Shen, *Carbon* 38 (2000) 789–795.
- [8] C.X. Pan, Y.L. Liu, F. Cao, J.B. Wang, Y.Y. Ren, *Micron* 35 (2004) 461–468.
- [9] A. Tanaka, S.H. Yoon, I. Mochida, *Carbon* 42 (2004) 1291–1298.
- [10] S. Sato, A. Kawabata, M. Nihei, Y. Awano, *Chem. Phys. Lett.* 382 (2003) 361–366.
- [11] M.H. Rummeli, F. Schäffel, C. Kramberger, T. Gemming, A. Bachmatiuk, R.J. Kalenczuk, B. Rellinghaus, B. Büchner, T. Pichler, *J. Am. Chem. Soc.* 129 (2007) 15772–15773.
- [12] S. Lim, S.H. Yoon, Y. Korai, I. Mochida, *Carbon* 42 (2004) 1765–1781.
- [13] M.J. Aus, B. Szpunar, U. Erb, A.M. El-Sherik, G. Palumbo, K.T. Aust, *J. Appl. Phys.* 75 (1994) 3632–3634.
- [14] A. Marlot, P. Kern, D. Landolt, *Electrochim. Acta* 48 (2002) 29–36.
- [15] N.S. Qu, D. Zhu, K.C. Chan, W.N. Lei, *Surf. Coat. Technol.* 168 (2003) 123–128.
- [16] R.T.C. Choo, J.M. Toguri, A.M. El-Sherik, U. Erb, *J. Appl. Electrochem.* 25 (1995) 384–403.
- [17] S.K. Ghosh, A.K. Grover, G.K. Dey, M.K. Totlani, *Surf. Coat. Technol.* 126 (2000) 48–63.
- [18] W.-C. Tsai, C.-C. Wan, Y.-Y. Wang, *J. Appl. Electrochem.* 32 (2002) 1371–1378.
- [19] Y.L. Liu, Q. Fu, C.X. Pan, *Carbon* 43 (2005) 2264–2271.
- [20] S. Tao, D.Y. Li, *Nanotechnology* 17 (2006) 65–78.
- [21] K.R. Murali, V. Swaminathan, D.C. Trivedi, *Sol. Energy Mater. Sol. Cells* 81 (2004) 113–118.
- [22] C. Suárez, E. Chávez, J.A. Díez, H. Grandel, R. Guixá, *Trans. Inst. Met. Finish.* 85 (2007) 46–50.
- [23] M. Chhowalla, K.B.K. Teo, C. Ducati, N.L. Rupasinghe, G.A.J. Amaratunga, A.C. Ferrari, D. Roy, J. Robertson, W.I. Milne, *J. Appl. Phys.* 90 (2001) 5308–5317.
- [24] F.L. Yuan, H.J. Ryu, *Nanotechnology* 15 (2004) S596–S602.
- [25] X. Qi, X.F. Ruan, C.X. Pan, *Mater. Lett.* 61 (2007) 4272–4275.
- [26] M. Kawaguchi, K. Nozaki, S. Motojima, H. Iwanaga, *J. Cryst. Growth* 118 (1992) 309–313.
- [27] X.Q. Chen, S. Motojima, *J. Mater. Sci.* 34 (1999) 5519–5524.
- [28] Y.K. Wen, Z.M. Shen, *Carbon* 39 (2001) 2369–2374.
- [29] D. Landolt, A. Marlot, *Surf. Coat. Technol.* 169–170 (2003) 8–13.
- [30] S.V. Meschel, O.J. Kleppa, *J. Alloys Compd.* 321 (2001) 183–200.
- [31] Y. Fukumiya, Y. Haga, O. Nittono, *Mater. Sci. Eng. A* 312 (2001) 248–252.
- [32] V.G. Kudin, V.A. Makara, *Inorg. Mater.* 41 (2005) 591–594.
- [33] J. Shi, O. Nittono, *J. Mater. Sci. Lett.* 11 (1992) 22–25.
- [34] S.S. Fan, M.G. Chapline, N.R. Franklin, T.W. Tomblor, A.M. Cassell, H.J. Dai, *Science* 283 (1999) 512–514.
- [35] C. Bower, O. Zhou, W. Zhu, D.J. Werder, S.H. Jin, *Appl. Phys. Lett.* 77 (2000) 2767–2769.